Mindin/spondin-2 regulates fibroblast subpopulations through distinct Src family kinases during fibrogenesis

Sunny Kataria[1,2,3], Isha Rana[1,4], Krithika Badarinath[1,3], Rania F Zaarour[1,&], Gaurav Kansagara[1,5], Sultan Ahmed[1], Abrar Rizvi[1], Dyuti Saha[1,5], Binita Dam[1,5], Abhik Dutta[1,4], Ravindra K Zirmire[1,4], Edries Yousaf Hajam[1,4], Pankaj Kumar[1], Akash Gulyani[6,@], Colin Jamora[1,2]

1 IFOM-inStem Joint Research Laboratory, Centre for Inflammation and Tissue Homeostasis, Institute for Stem Cell Science and Regenerative Medicine (inStem), Bangalore, Karnataka, India.

2. Department of Life Sciences, Shiv Nadar Institution of Eminence, Gautam Buddha Nagar, India

3 National Centre for Biological Sciences (TIFR), GKVK Post, Bangalore, Karnataka, India.

4 Shanmugha Arts, Science, Technology and Research Academy (SASTRA) University, Thanjavur, Tamil Nadu, India.

5 Manipal Academy of Higher Education, Manipal, India.

6 Integrative Chemical Biology, Institute for Stem Cell Science and Regenerative Medicine (inStem), Bangalore, Karnataka 560065, India

* Corresponding author: Colin Jamora, Department of Life Sciences, Room B122C (B Block), Shiv Nadar University, NH-91, Tehsil Dadri, District Gautam Buddha Nagar, Uttar Pradesh 201314, India, Tel: +91 120-7170100 (ext 183), colin.jamora@snu.edu.in

& Current address: Thumbay Research Institute for Precision Medicine, Gulf Medical University, Ajman, UAE

@ Current address: Department of Biochemistry, School of Life Sciences, University of Hyderabad, Central University Post, Prof. C.R. Rao, Gachibowli, Hyderabad, Telangana 500046, India

Conflict of interest: The authors declare no conflict of interest

ABSTRACT

Fibrosis results from excessive extracellular matrix (ECM) deposition, causing tissue stiffening and organ dysfunction. Activated fibroblasts, central to fibrosis, exhibit increased migration, proliferation, contraction, and ECM production. However, it remains unclear if the same fibroblast performs all of the processes that fall under the umbrella term of "activation". Due to fibroblast heterogeneity in connective tissues, subpopulations with specific functions may operate under distinct regulatory controls. Using a transgenic mouse model of skin fibrosis, we found that Mindin (spondin-2), secreted by *Snail transgenic* keratinocytes, differentially regulates fibroblast subpopulations. Mindin promotes migration and inflammatory gene expression in SCA1+ dermal fibroblasts via Fyn kinase. In contrast, it enhances contractility and collagen production in papillary CD26+ fibroblasts through c-Src signalling. Moreover, in the context of the fibrotic microenvironment of the tumour stroma, we found that differential responses of resident fibroblasts subpopulations to Mindin extend to the generation of functionally heterogeneous cancer-associated fibroblasts (CAFs). This study unveils Mindin as a key orchestrator of dermal fibroblast heterogeneity, reshaping cellular dynamics and signalling diversity in the complex landscapes of skin fibrosis and cancer.

INTRODUCTION

Fibrosis is a leading cause of death in many chronic diseases and the central players in this pathophysiology are fibroblasts. The key events in its pathogenesis can be conceptualized as a chronic exaggeration of wound-healing processes that lead to scarring (1–3). The processes involved in wound healing can be broadly divided into four overlapping phases – hemostasis, inflammation, proliferation, and remodelling (4). During the inflammatory phase, the fibroblasts are activated and migrate to the site of injury. The fibroblasts at the wound site proliferate and differentiate into myofibroblasts, where they perform several functions and coordinate multiple aspects of the wound-healing program (5). While the number of activated fibroblasts dissipates following normal wound healing, this is not the case with fibrotic diseases, which are associated with the persistent presence of activated fibroblasts (5, 6). However, to understand what causes the persistence of activated fibroblasts in pathological scenarios such as fibrosis, it is important to understand what activates them and how they remain in a chronically active state.

A major complication in understanding fibroblast regulation and function is that fibroblasts in the dermal compartment of the skin are spatially and functionally heterogeneous (7–9). Fibroblasts in the neonatal skin arise from two distinct lineages. The upper lineage, marked by CD26, forms the papillary dermis and contributes to hair follicle generation, arrector pili muscle, and epidermal homeostasis (8, 9). The lower dermal lineage, marked by SCA1SCA1, contributes to the deposition of the majority of fibrous collagen and can differentiate into adipocytes to maintain the dermal white adipose layer (8–10). In wound healing, the SCA1SCA1^{+} fibroblasts are the first cells recruited to the wound bed where they repopulate the ECM, while recruitment of papillary fibroblasts is associated with re-epithelialisation and hair follicle generation (9).

These subpopulations also display heterogeneous responses in fibrosis (10–13). Nonetheless, the contributions of various fibroblast subpopulations in response to pro-fibrotic stimuli and the molecular mechanisms underlying their differential activities remain largely unknown. To begin uncovering these molecular mechanisms, we utilised a *Snail transgenic (Snail Tg)* mouse model of skin fibrosis that mimics the overexpression of this transcription factor found in the epidermis of scleroderma (SSc) patients (14, 15). Ectopic expression of snail is sufficient to induce phenotypes that recapitulate many diagnostic features of systemic scleroderma including dermal thickening and fibrosis (15). It is also interesting to note that scleroderma patients also have a higher incidence of developing cancers (16), suggesting that insights into this fibrotic disease would likewise shed light on the factors driving tumorigenesis. In line with this, the *Snail Tg* mice have also been shown to prime the skin towards the development of cutaneous squamous cell carcinoma (17, 18).

The mesenchymal compartment of fibrotic tissue has remarkable similarities to the stroma surrounding solid tumours (19, 20). The fibrosis associated with tumour stroma is driven by cancer-associated fibroblasts (CAFs) (21). Much like their counterparts in normal tissue, CAFs are heterogeneous in nature (20). One subpopulation of CAFs, known as myofibroblastic CAFs (myCAFs), expresses higher levels of alpha-Smooth Muscle Actin (aSMA), collagens and other genes associated with myofibroblast functions (22). Another major subpopulation is the inflammatory CAFs (iCAFs) which majorly express inflammatory cytokines (22). Collectively, these different CAFs promote tumour-associated inflammation, regulate ECM-remodelling of stroma, regulate cancer cell metabolism, promote survival and maintenance of cancer stem cells, and aid metastasis and chemoresistance (19, 20). Despite their important contributions to tumorigenesis, the origins of these different CAFs remain unanswered. We have previously shown that *Snail Tg* keratinocytes secrete Mindin (Spondin-2; a member of the F-Spondin family) (18). Mindin has been implicated in response to injury (23, 24) and is overexpressed in multiple inflammatory and fibrotic diseases (25–30). It has also emerged as a prognostic and diagnostic biomarker for various carcinomas

(31–35) and we have previously shown that Mindin is essential for tumorigenesis and fibrogenesis in the *Snail Tg* mouse model (15, 18). This presented us with a unique opportunity to further investigate the role of Mindin in elucidating the regulation of the functional heterogeneity of fibroblasts in both tissue fibrosis and the tumour stroma.

RESULTS

The *Snail Transgenic (Snail Tg)* skin has perturbed proportions and localisation of fibroblast subpopulations.

We have previously shown that aSMA, a marker for activated fibroblasts, is upregulated in the *Snail Tg* dermis as early as postnatal day 9 (36). The dermal fibroblasts can be spatially subdivided into two major subpopulations, papillary fibroblasts in the upper dermis and reticular and hypodermal fibroblasts in the lower dermis (37, 38). These subpopulations can be isolated based on surface markers, CD26 for papillary and SCA1SCA1 for lower reticular/hypodermal fibroblasts (8–10). The parameters of fibroblast heterogeneity, such as the proportion of specific fibroblast subtypes, may be altered during repair and disease conditions (39). To determine the proportions of fibroblast subpopulations we performed flow cytometry using high vimentin (VIM) expression as a classical marker for fibroblasts (40,41). We observed a significant increase in the proportion of VIM^{high} cells that expressed SCA1SCA1 (lower dermal fibroblasts), while the proportion of VIM^{high} cells that express CD26 but not SCA1SCA1 (papillary fibroblasts) showed a small decrease of ~1% in the *Snail Tg* skin (Figure S1A-S1E). In addition, there was no significant change in the VIM^{high} cells expressing both CD26 and SCA1SCA1 in the *Snail Tg* skin (Figure S1F). However, the pool of VIM^{high} fibroblasts that did not express SCA1SCA1 and CD26 ($SCA1SCA1^{-}CD26^{-}$) was decreased (Figure S1G) and this suggests that this pool can possibly be the source for the increase in lower dermal fibroblasts ($SCA1SCA1^{+}CD26^{-}/VIM^{high}$) in the *Snail Tg* skin. Moreover, we observed that non-fibroblasts (VIM^{-}) expressing either SCA1SCA1 or CD26 were unchanged in the *Snail transgenic* background (Figure S1H-S1I). We probed for the expression of aSMA in $CD26^{+}/SCA1SCA1^{-}/VIM^{high}$ and $SCA1SCA1^{+}/CD26^{-}/VIM^{high}$ cells to determine the activation status of these two subpopulations of fibroblasts. Both subpopulations showed an increase in the number of activated cells in the *Snail Tg* background relative to its wild-type (WT) control (Figure 1A-1D; Supplementary Table 1). Altogether, this demonstrates that in the *Snail Tg* background, the proportions of fibroblast subpopulations are perturbed and both subpopulations contribute to the pool of activated cells.

Interestingly, when we investigated the spatial organisation of the cells in vivo, we found that $SCA1SCA1^{+}$ fibroblasts are progressively recruited from the lower dermis to the epidermal-dermal junction (Figure 1E-1F, S1J-S1K). Analysis of the probability distribution of $SCA1SCA1^{+}$ fibroblasts as a function of distance from the epidermis revealed that $SCA1SCA1^{+}$ cells were distributed between 50-150 μm away from the epidermis in WT skin at all postnatal ages analysed (Figure 1F and Figure S1K). In the *Snail Tg* skin, the $SCA1SCA1^{+}$ cells are first noticed to have a differential localisation at P5, and the probability of finding these cells near the epidermis gradually increases over time. Interestingly, the papillary localisation $CD26^{+}$ fibroblasts between the WT and *Snail Tg* skin remain largely invariant (Figure 1G-1H, S1L-S1M).

Mindin induces migration of SCA1SCA1^{+} fibroblasts

We recently observed that the matricellular protein Mindin is secreted from *Snail Tg* keratinocytes (15, 18) and is required for the expression of inflammatory cytokines in dermal fibroblasts (15). Mindin was also found to be necessary for dermal thickening, as measured by H&E staining, and for fibrosis, as indicated by collagen 1 levels in the transgenic mouse(15). In addition, we found that Mindin deficiency reduced the number of activated dermal fibroblasts marked by aSMA in *Snail Tg/Min KO* (*Mindin knockout*) skin (Figure S2A-B) To test whether Mindin is also required for the relocalisation of SCA1^{+} fibroblast towards the epidermal-dermal junction in the *Snail Tg* skin, we stained SCA1^{+} fibroblasts (Figure 2A) and quantified their localisation in P9 WT, *Snail Tg*, and *Snail Tg/Min KO* skin (Figure 2B, S2C). The localisation of SCA1^{+} cells in the *Snail Tg/Min KO* was similar to WT skin, indicating that Mindin is required for the relocalisation of the cells from the lower dermis toward the epidermal-dermal junction. Furthermore, conditioned media from a Mindin-expressing CHO cell line induced migration of fibroblasts in vitro whereas the control CHO-conditioned media had no effect (Figure S2D-E). To test whether Mindin is sufficient to change SCA1^{+} fibroblast localisation, we assessed if purified recombinant Mindin can function as a chemoattractant in vitro (Figure S2F-G). For this purpose, we sorted and cultured CD26^{+} and SCA1^{+} fibroblasts and seeded them in a transwell chamber. Upon addition of Mindin to the lower chamber of the transwell SCA1^{+}, but not the CD26^{+} cells, migrated in this assay (Figure 2C), indicating that the chemotactic response to Mindin is unique to the SCA1^{+} fibroblasts.

To gain insights into the molecular mechanisms underlying the pro-migratory effect of Mindin on fibroblasts, we performed gene set enrichment analysis (GSEA) on differentially upregulated genes (1715 upregulated genes with $q<0.05$, FC>1.5 folds; Supplementary Table 2) from RNAseq data of Mindin-treated fibroblasts (15). The analysis revealed significant enrichment in biological processes (Supplementary Table 3) associated with cell migration (41 genes) and positive regulation of cell migration (45 genes) (Figure S2H). We created a sublist of 81 upregulated genes associated with these processes and reperformed GSEA. We found enrichment in processes associated with the cytoskeletal organisation, cell adhesion, and ECM organisation, along with the activation of integrin signalling and kinases involved in cell migration (Figure S2I). Mindin is a known integrin ligand (40–42)[31–33], and we hypothesised that Mindin might activate the src family of Kinases (SFK), given that the integrin-SFK axis has previously been reported to mediate fibroblast migration (43–45). To test whether Mindin exposure activates SFK in dermal fibroblasts, we probed for phospho-SRC (pSRC) levels via western blot. We observed that Mindin was able to activate src family kinases within 15 minutes of treatment (Figure 2D and S2J). To assess whether the activation of src family kinases by Mindin is necessary for the migration of SCA1^{+} fibroblasts, we used two different SFK inhibitors - pp2 (pan SFK inhibitor) (46, 47) and KbSrc4 (a preferential inhibitor of c-SRC) (48). While the addition of pp2 to the transwell chamber inhibited the migration of SCA1^{+} cells, this was not the case with KbSrc4 (Figure 2E). Given that KbSrc4 is more potent in inhibiting c-SRC over other SFK members such as FYN and YES (48), this suggested a differential role of SFK members in mediating the effect of Mindin. Thus, to delineate this further, we generated shRNA-based knockdowns of *Src*, *Fyn* and *Yes* kinases which showed a 60-80% reduction in RNA expression of *Src*, *Fyn* and *Yes*, respectively (Figure S2K). In a transwell migration assay, SCA1^{+} cells transduced with non-targeting shRNA, Src shRNA and Yes shRNA migrated in response to Mindin, but cells transduced with Fyn shRNA did not (Figure 2F). This indicated a non-redundant essential role of *Fyn* in the migration of SCA1^{+} fibroblasts downstream of Mindin.

We then investigated whether this phenomenon is characteristic of a physiological process such as wound healing. It has been previously shown that lower dermal fibroblasts

(expressing SCA1) migrate into the wound bed at early stages followed by upper dermal fibroblasts in later stages (9). Given the evidence for the role of Mindin in fibroblast migration, we investigated whether Mindin is also important for the localisation/recruitment of SCA1$^+$ fibroblasts in wound healing. We wounded WT mice and quantified the expression of Mindin RNA in the wounded skin from day-1 to day-10 post wounding. We observed that Mindin expression starts increasing from day-3 post-wounding, peaks at day-7 and decreases thereafter (Figure S2L). We, therefore, stained the wounded skin for SCA1$^+$ cells on day-7 and day-9 post wounding. Immunofluorescence staining of day-7 and day-9 post-wounded skin revealed decreased numbers of SCA1$^+$ cells localised in the wound bed in *Min KO* compared to WT mice (Figure 2G-H) consistent with a defect in Sca-1 migration in the absence of Mindin. In line with the importance of lower dermal fibroblasts in the wound healing response (9), the failure to recruit SCA1+ cells into the wound bed corresponded to a delay in wound closure during the post-wounding day 7 to day 9 timeframe (Figure 2I).

Mindin induces an inflammatory phenotype in SCA1$^+$ fibroblasts

We have previously reported that there is robust inflammation in the *Snail Tg* skin (36, 49), which is substantially decreased in the absence of Mindin (15). In addition, we now observe that purified Mindin is sufficient to induce inflammatory cytokine expression in fibroblasts in vitro (Supplementary Table 2-3). This data is further supported by increased production of IL1b and IL6 cytokines upon treatment of fibroblasts with Mindin, as observed via ELISA (Figure S3A). We then analysed which fibroblast subpopulation was responsive to Mindin to induce an inflammatory response. Thus, we treated the sorted population with purified recombinant Mindin in vitro and quantified the expression of various cytokines, which were observed to be differentially upregulated in the RNAseq analysis of Mindin-treated fibroblasts. In CD26$^+$ fibroblasts, Mindin did not cause significant upregulation of most inflammatory cytokines, but there was a small but significant increase in IL6 expression (Figure 3A). On the other hand, Mindin-treated SCA1$^+$ cells exhibited a robust upregulation of all the cytokines we analyzed (Figure 3B). Furthermore, CXCL-3, which was undetected in CD26$^+$ fibroblasts, was expressed in SCA1$^+$ fibroblasts and showed a robust increase in response to Mindin. This data indicates that Mindin is sufficient to strongly induce the expression of pro-inflammatory cytokines preferentially in SCA1$^+$ fibroblasts. To validate if SCA1$^+$ fibroblasts were indeed the dominant producers of inflammatory cytokines, we removed other CD26 and SCA1 expressing cells in the skin, such as hematopoietic cells (CD45) and endothelial cells (CD31). All cytokines tested except IL6 were significantly increased in SCA1$^+$ fibroblasts isolated from *Snail Tg* skin (Figure S3B). *Cxcl10* increased in both CD26+ and SCA1$^+$ subpopulations, however, SCA1$^+$ fibroblasts from *Snail Tg* skin expressed higher levels of *Cxcl10* compared to CD26$^+$ fibroblasts (Figure S3B).

We then focused on the mechanism by which extracellular Mindin can stimulate cytokine gene expression. Given that Mindin has been previously shown to activate the NFkB pathway in renal cells (HK-2 cells) (26), and NF-kB is known to be important for inflammatory cytokine expression in multiple cell types including fibroblasts (50–56). In line with this, we found the NFkB pathway as one of the KEGG pathways enriched in the GSEA in Mindin-treated fibroblasts (Figure S3C; Supplementary Table 4). Moreover, the majority of SCA1$^+$ cells demonstrated a nuclear translocation of NFkB upon one hour of Mindin treatment (Figure 3C-E and S3D-E).

Given our observation that there is a deficiency of SCA1$^+$ cells in the wound bed on day 7 post-wounding, we predicted that *Mindin KO* wounds would also have a deficiency in recruiting immune cells into the wound bed. Consistent with this prediction, staining of day-7 wound sections revealed a reduced number of T-cells in the wound beds of Mindin null animals, though macrophages (detected by either CD11b or F4/80) were largely unaffected (Figure 3F-H, S3F-G).

Mindin induces collagen contraction in CD26$^+$ fibroblasts in a c-Src-dependent manner

Though there was not an obvious perturbation in the localisation of CD26$^+$ fibroblasts, a qualitative change in both a denser packing and a more uniform orientation of papillary fibroblasts was observed in the *Snail Tg* skin, which was lost in the absence of Mindin (Figure S4A). To test whether there is denser packing of the papillary fibroblasts, the distance between two neighbouring CD26$^+$ cells was measured and plotted as a function of the distance from the epidermis (Figure 4A). In agreement with the qualitative observation, the quantification revealed a significant reduction in the intracellular distance between neighbouring CD26$^+$ cells in *Snail Tg* mice closer to the epidermis. Nevertheless, in *Snail Tg/Min KO* mice, the dense packaging of CD26$^+$ cells was attenuated. Many factors can influence the density of cells in the dermis, one of which is the increased number of CD26$^+$ cells in the *Snail transgenic* background. However, there was no difference in the proportion of papillary fibroblasts in the WT vs *Snail Tg* skin (Figure S1B-E). Another possibility is that myofibroblast contraction may result in the compaction of the matrix resulting in an increased localised density of cells. Furthermore, fibroblasts in contracting gels become parallelly aligned and are closely packed together (57). Hence, we hypothesised that CD26$^+$ fibroblasts might differentiate to contractile myofibroblasts in the *Snail Tg* skin in a Mindin-dependent fashion. To test this hypothesis, heterogeneous fibroblasts and FACS-sorted SCA1$^{+,}$ and CD26$^+$ fibroblasts were embedded in collagen gels and treated with Mindin. 72-hours post-treatment, we measured the area of the treated gels and found that Mindin can promote collagen contraction in gels seeded with either mixed fibroblasts or CD26$^+$ fibroblasts (Figure 4B and S4B). However, this was not the case for SCA1$^+$ fibroblasts.

We then investigated the mechanism by which Mindin can induce contraction in CD26$^+$ fibroblasts. The src family of kinases has been shown to be involved in the regulation of myofibroblast differentiation and contraction downstream of TGFb1 (58). The integrin-src signalling axis has been implicated in the regulation of RhoA-ROCK activation, which can affect stress fibre formation and contractile activity via myosin light chain phosphorylation (59). Given our observation that Fyn kinase drives the migration of SCA1$^+$ cells in response to Mindin, we investigated whether SFKs are also necessary for Mindin-induced contraction of CD26$^+$ cells. Both the pan-SFK inhibitor PP2 as well as the c-SRC specific inhibitor, KbSrc4, blocked Mindin-mediated contraction (Figure 4C and S4C). To further access which member of the SFK was required for the contraction of CD26$^+$ cells, we knocked down *Src*, *Fyn* and *Yes* kinases by transduction of specific shRNAs. The transduced cells were embedded in collagen gels and treated with Mindin. While CD26$^+$ fibroblasts transduced with either non-targeting, Fyn or Yes shRNA contracted the collagen gels in response to Mindin, reduction of c-SRC inhibited the Mindin-mediated contraction (Figure 4D and S4D). This indicated that specific src family kinase members are differentially utilised for different aspects of fibroblast activation.

One of the physiological roles of fibroblast contraction is its contribution to the contraction of the wound bed, which aids in wound closure. Since we observed a delay in wound healing in Mindin null animals (Figure 2I), we calculated the rate of wound closure (as measured by the %closure/day) in WT and *Min KO* wounds as a proxy for in vivo tissue contraction. Our results show that contraction in WT mice starts on day 5 and continues until day 7 post-wounding. Interestingly, the magnitude of the contraction is lower in the *Min KO* animal (Figure 4E). However, unlike SCA1$^+$ cells, we did not observe any deficiency in the recruitment of CD26$^+$ fibroblasts in the wound bed of *Min KO* animals (Figure S4E-F). This indicates that while Mindin is not required for the migration and recruitment of CD26$^+$ cells, it plays a role in the contraction of the wounds.

Apart from contraction, another consequence of fibroblast activation is the increase in collagen production. Thus, to test if Mindin can affect collagen production, we treated the sorted fibroblasts with Mindin and measured the levels of Collagen 1 (COL1A1 and COL1A2) via western blot (Figure 4F and S4G). Only $CD26^+$ cells exhibited an increase in the amount of COL1 levels upon treatment with Mindin. Though COL1 is the most abundant collagen and contributor to tissue fibrosis, there are other collagens which play important roles in this pathology such as COL3, COL4, COL5, and COL7 (60, 61). The type of collagen upregulated may differ by the ligand and fibroblast subtype. Therefore, to test if Mindin differentially regulates the expression of collagen sub-types in $CD26^+$ and $SCA1^+$, we measured the mRNA expression level of these collagens via qPCR. *Col1a2*, *Col3a1*, and *Col5a* were significantly upregulated in Mindin-treated $CD26^+$ cells (Figure S4H, left panel). Interestingly, *Col3a1* was also significantly increased in Mindin-treated $SCA1^+$ cells (Figure S4H, right panel). These results reveal how different fibroblast subpopulations contribute in a complementary fashion to the overall increase in the bulk amount of collagen proteins in the fibrotic tissue.

Mindin promotes a CAF-associated self-renewal promoting capability in $CD26^+$ fibroblasts

The mesenchymal compartment of fibrotic tissues shares remarkable similarities with the stroma surrounding solid tumours (19,20). We thus hypothesized that Mindin might play a role in the generation of cancer-associated fibroblasts (CAFs), which are crucial in tumorigenesis (20,22). Supporting the potential role of Mindin in other fibrotic scenarios, such as solid tumours, there are reports of Mindin being upregulated in many cancers, where it is proposed as a potential diagnostic and prognostic biomarker (31–35). Furthermore, gene set enrichment analysis using Mindin-upregulated genes in fibroblasts revealed a significant enrichment of disease terms in the DisGeNET database for inflammatory and fibrotic diseases, as well as cancers (Figure S5A-S5B).

As shown in Figure 3A-B, Mindin differentially primes $SCA1^+$ fibroblast to adopt an inflammatory phenotype, consistent with iCAFs, which have also been shown to express *IL6, CCL5, CXCL12, CXCL10,* and *CXCL3* (22, 62, 63). Similarly, treatment with Mindin induces $CD26^+$ fibroblasts to become more contractile and secrete elevated levels of collagen (Figure 4B and 4F), which is characteristic of a myCAF phenotype (22). To test whether this is supported by molecular markers, we analysed the expression levels of signature genes of myCAFs (*aSma*, *Tagln*, *Mcam*, *Myh11*, *Myl6*, *Antrx1*, *Sema3c*, *Itga11*) (62, 63) in Mindin treated $CD26^+$ and $SCA1^+$ fibroblasts. While α-SMA expression was increased in both subpopulations treated with Mindin, other reported myCAF markers were significantly elevated only in Mindin-treated $CD26^+$ cells (Figure 5A-B). Furthermore, it has been shown that CD10, C5a, and GPR77 are signatures of a subset of CAFs in breast and lung cancer patients (64). Interestingly, only $CD26^+$ fibroblasts increased expression levels of *Gpr77* and C5a upon Mindin treatment, though there was no effect on CD10 expression (Figure 5C-D). C5a binds to its receptor GPR77, which activates NFkB in a positive feedback loop to further increase the expression of *GPR77* (64). In line with this, we found that prolonged treatment of $CD26^+$ fibroblasts with Mindin can activate NFkB signalling in these cells (Figure S5C-D).

An important function of myCAFs is the maintenance of cancer stem cells (CSCs) and chemoresistance, which is associated with poor prognosis (64). We then tested whether Mindin-treated fibroblasts are functionally equivalent to myCAFs and, in particular, capable of promoting the self-renewal of epithelial progenitor/stem cells. For this purpose, we co-

cultured primary mouse epidermal keratinocytes (mKTs) with CD26$^+$ or SCA1$^+$ fibroblasts pre-treated with either buffer or Mindin and measured self-renewal using a colony formation assay. Only Mindin-treated CD26$^+$ fibroblasts were able to increase colony formation of mKTs (Figure 5E). Furthermore, culturing mKTs in conditioned media (CM) collected from Mindin-treated CD26$^+$ fibroblasts was sufficient to increase colony formation (Figure 5F), indicating a role of molecular crosstalk between CD26$^+$ dermal fibroblasts and keratinocytes via soluble factors.

DISCUSSION

Our data reveal Mindin as a modulator of heterogeneous dermal fibroblasts that drive cutaneous fibrogenesis (Figure 5G). We have shown that Mindin, secreted by *Snail Tg* keratinocytes (18), elicits unique functional responses in resident subpopulations of fibroblasts in the skin. Mindin mediates the migration of SCA1$^+$ fibroblasts via Fyn kinase and increases inflammatory cytokine production in these cells. Conversely, Mindin induces a more contractile phenotype in CD26$^+$ fibroblasts and increases collagen 1 production. However, Mindin utilises c-Src to mediate this effect in papillary fibroblasts. Interestingly, the effect of Mindin on SCA1$^+$ and CD26$^+$ fibroblasts endow them with features of iCAFs and myCAFs, respectively. Additionally, Mindin-treated CD26$^+$ fibroblasts can promote self-renewal of epithelial cells, akin to the role of myCAFs in maintaining cancer stem cells. This data is consistent with the notion that CAFs can be derived from resident fibroblasts within the tissue (65, 66). Furthermore, we have previously analysed published datasets of various fibrotic models and observed that Mindin is also overexpressed in bleomycin-induced fibrosis in skin and lungs, UUO (Unilateral Ureteral Obstruction) kidney fibrosis model and high-fat diet-induced NASH (Nonalcoholic steatohepatitis) model (15). This suggests that the role of Mindin may not be limited to *Snail Tg* mice but could extend to other fibrotic mouse models and tissues. Fibroblast heterogeneity has also been reported in the human skin. Single-cell RNAseq has revealed that human dermal fibroblasts can be categorized into four subgroups, namely - mesenchymal, inflammatory, secretory papillary and secretory reticular (67). In fibrotic conditions such as keloids and scleroderma, specific markers for each subpopulation are differentially regulated (68). Notably, we found a significant overlap with the markers of these subpopulations in Mindin-treated human dermal fibroblasts (Figure S6A). We found that the spatial organisation of SCA1$^+$ cells is perturbed in the *Snail transgenic* background and have attributed Mindin-mediated migration as an underlying cause. Besides cellular migration, another possible explanation is the transdifferentiation of CD26+ cells into SCA1+ fibroblasts. One prediction of a transdifferentiating CD26$^+$ to SCA1$^+$ fibroblast would be the detection of a transitional state of the cell where they would be double-positive for both markers. However, both wild-type and *Snail transgenic* skin contained only a small percentage of fibroblasts that were double-positive for CD26 and SCA1 (Figure S1C and S1F), which cannot explain the increased number of SCA1$^+$ cells at the dermal-epidermal junction in the transgenic animal. Additionally, treatment with Mindin did not induce expression of SCA1 in CD26$^+$ fibroblasts nor vice versa (Figure S6B). It should be noted that SCA1 is also expressed on endothelial cells (marked by CD31) and some hematopoietic cells (marked by CD45). However, CD45$^-$CD31$^-$SCA1$^+$ cells were more predominant in the total cell population and showed an increase in *Snail Tg* skin, while CD45$^+$CD31$^+$SCA1+ did not significantly change in the *Snail Tg* skin (Supplementary Table 5). This makes the hematopoietic compartment or endothelial cells an unlikely source for the increased proportion of SCA1$^+$ cells. SCA1$^+$ fibroblasts have been reported to express pre-adipocyte markers and contribute to the maintenance of adipose tissue homeostasis (8–10). A functional consequence of relocating the SCA1$^+$ fibroblasts from the lower to the upper dermis is the deprivation of a potential source of adipose tissue that lies within the lower dermis. Consistent with this, in the adult *Snail transgenic* skin, there is a near-total absence of dermal white adipose tissue that is replaced by collagen(15).

One notable observation was the increase in the number of SCA1$^+$ fibroblasts in the *Snail transgenic* skin (Figure S1A and S1D) without an increase in proliferation (Figure S6C). This increase may be possible through the inhibition of SCA1$^+$ fibroblasts differentiating into other lineages. As noted earlier, under homeostatic conditions, SCA1$^+$ fibroblasts differentiate to maintain adipose tissue homeostasis (9). However, β-catenin stabilisation in SCA1$^+$ fibroblasts has been shown to inhibit their differentiation into adipocytes, thereby promoting fibrosis (8). Our results indicate that Mindin treatment activates β-catenin signalling in SCA1$^+$ fibroblasts in-vitro, as measured by an increase in the β-catenin target gene *Axin2* (Figure S6D). This suggests that the increase in SCA1$^+$ cells in the *Snail transgenic* skin is at least partly due to an accumulation of cells that do not otherwise differentiate into adipocytes. However, inhibition of β-catenin using the iCRT5 inhibitor (69) did not inhibit Mindin-mediated migration (Figure S6E). Nevertheless, it cannot be ruled out that other fibroblast subpopulations, such as Dlk$^+$SCA1$^-$ reticular fibroblasts, which have been shown to contribute to all compartments of the dermis (9) do not contribute to the SCA1$^+$ population in *Snail Tg* mice.

It has been shown that lower dermal fibroblasts are the major source of fibrous collagen during homeostasis and physiological repair (37, 38). Nevertheless, we observed that it was the papillary fibroblasts which increased the levels of Col1 in response to Mindin. This suggests that in fibrotic scenarios, CD26$^+$ cells can be induced to provide a substantial amount of ECM proteins. This is consistent with the report by Rinkevich et al., 2015 (11) that En1$^+$ derived CD26$^+$ fibroblasts constitute the major population with fibrogenic potential, and a CD26 inhibitor inhibits scarring.

In addition to stimulating a local contracture, the ordered packaging of CD26$^+$ papillary fibroblasts is also consistent with the alignment of myCAFs observed immediately adjacent to carcinomas (70). This packaging can arise from the contractile forces exerted on the matrix by myCAFs and the remodelling of the local ECM (70). Along with showing features consistent with myCAFs, the papillary fibroblasts are also located in a histological position consistent with the origins of myCAFs.

Altogether, these findings provide new insights into the heterogeneous regulation of fibrosis-associated and cancer-associated fibroblasts, and many interesting questions remain to be resolved. For instance, the differential response of fibroblast subpopulations corresponding to different members of SFKs may hint at the differential expression of cognate Mindin receptors in these cells. These differences may be at the level of surface expression of distinct integrin pairs (which have been shown to act as receptors for Mindin on macrophages, T-cells and colorectal cancer (40, 41, 71)) and/or different cytoplasmic machinery downstream of the receptors. The differences may also arise owing to distinct levels and/or localization of SFK members or their adaptor molecules in different fibroblasts. Our transcriptomic data (Supplementary Table 2) did reveal differential expression of Fyn upon Mindin treatment. These possibilities should thus be explored in future studies. Furthermore, there are additional fibroblast subpopulations that may contribute to fibrotic tissue and were not addressed in this study. These include Dlk$^-$SCA1$^-$ reticular fibroblasts, pericytes, fibrocytes, and MSCs. Moreover, further refinement of these SCA1$^+$ and CD26$^+$ subpopulations and their responses to different pro-fibrotic stimuli may shed light on the pathophysiology of fibrosis and the tumour stroma. For example, myCAFs have been reported to be a double-edged sword, capable of both promoting (22) and restraining tumours (72). Thus, it would be interesting to determine if refinement of the CD26$^+$ subpopulation can explain the two opposing phenotypes or if the same subpopulation can switch the phenotype in response to different microenvironmental compositions.

METHODS

Sex as a biological variable

Our study examined both male and female animals, and similar results were observed for both sexes.

Animal studies

C57Bl6 (WT) mice were obtained from The Jackson Laboratory (Bar Harbor, Maine*), Mindin KO* mice were obtained from You-Wen He (Duke University, Durham, NC), and the *Snail Tg* mouse was engineered as described earlier (14). The K14-Snail Tg/Mindin KO mouse was developed by breeding the *K14-Snail Tg* and *Mindin KO* mice.

Cell culture

Primary newborn dermal fibroblasts (NBDF; Mixed fibroblasts) isolation was performed as described earlier (36) from C57Bl6 postnatal day 2 (P2)- day 3 (P3) pups. Human primary dermal fibroblasts were procured from ScienCell Research Laboratories (Cat# 2320). All fibroblasts were cultured in DMEM high glucose media with 10% FBS. All experiments were performed on fibroblasts in between passages #2-#5. Primary mouse epidermal keratinocytes were harvested from the P2/P3 epidermis and cultured in low calcium E-media to maintain an undifferentiated proliferating state as previously described (73, 74). Further details on the sorting and culture of CD26 and SCA1 fibroblasts are provided in supplementary methods.

Mindin purification and treatment

Histidine-tagged Mindin was purified from conditioned media collected from CHO-Mindin cells (which was a generous gift from You-Wen He of the School of Medicine, Duke University) using Ni-NTA beads (Thermo Fisher Scientific) according to the manufacturer's protocol. Buffers with varying strengths of imidazole were made in 10 mM Tris and 300 mM NaCl (pH = 8) for washing and elution. The purified Mindin (10ml) was dialysed in for 3 rounds in 1L dialysis buffer (10mM tris. 20mM NaCl, pH = 8), concentrated using 10 kDa Centricon concentrator, and filtered with a 0.2 µm syringe filter. Silver staining and western blot using Mindin antibody (Santa Cruz SC49050 at dilution 1:100 & Jackson ImmunoResearch 705-035-147 secondary at dilution 1:200) were performed to assess the purity and confirm the purification of Mindin. The purified recombinant Mindin was used at a concentration of 80-200 ng/ml in all treatments. All treatments were done in serum-free conditions unless otherwise stated.

Fluorescence-activated cell analysis

The detailed flow cytometry method is described in supplementary methods.

Lentiviral transductions

All lentiviral production and transductions were done in a BSL-2 facility in accordance with approved IBSC protocols. The method for lentiviral particle generation and the shRNA-pZip-mEf1a plasmids for *c-Src*, *Fyn* and *Yes* shRNA (procured from transomics) have been described earlier [21]. The titre of the virus that yielded greater than 50% GFP^+ cells was used to transduce sorted $SCA1^+$ or $CD26^+$ fibroblasts after the first passage, at 70-80% confluency. 72 hours post-infection, the virus-containing media was removed, and fresh

media with 1 µg/ml puromycin was added to enrich transduced cells. Plates showing greater than 90% GFP^+ cells were used for further experiments.

Transwell migration assay

The detailed methodology for transwell migration assay is described in supplementary methods.

Collagen contraction assay

Collagen contraction assay was done as previously described (15, 75) with NBDF, SCA1+, CD26+ or shRNA transduced fibroblasts. The detailed protocol is described in supplementary methods.

Western blot

Cells were serum-starved overnight before treatment and were treated with either buffer or Mindin in a serum-free medium for 15 minutes. Cells were lysed in RIPA buffer and were loaded after the addition of Laemmli buffer. The membranes were probed for phosphorylated SRC (pSSRC; CST 2101) and then with total SRC (SRC; CST2123) after stripping. For assessment of collagen 1, serum-starved cells are treated with either buffer or Mindin for 48-hours. Cells were lysed in RIPA, and the lysates were loaded in the gels along with Laemmli buffer. The membranes were probed with anti-collagen antibodies (Abcam ab21286) and Lamin B (Abcam AB16048). The HRP-labelled secondary antibodies (Jackson ImmunoResearch 305-035-003) were used at 1:3,000 dilution. Blots were developed on an ImageQuant LAS4000, and bands were quantified using Fiji software (ImageJ, NIH).

Cell localisation analysis

The detailed methodology for cell localisation analysis is described in the supplementary methods.

Nearest neighbour analysis

The detailed methodology for nearest neighbour analysis is described in the supplementary methods.

Colony formation

The detailed methodology for colony formation is described in the supplementary methods.

Wound healing

Two excisional wounds (separated by 1-1.5) cm were created on the mid-dorsal skin of the anaesthetised 3-4-month-old mice. Pictures were taken from day-1 to day-10 post wounding. Percent wound closure was calculated as $C = (1 - W_n/W_1)*100$, where C is percent wound closure, W_n is wound area on day n, and W_1 is wound area on day 1. The slope or rate of wound closure was determined as % closure/day, $R = C_n - C_{n-1}$, where C_n is % closure on a given day n and C_{n-1} is % closure on the previous day. Mice were sacrificed, and wounds were harvested on day-0 (unwounded) and days 3, 5, 7, 9, and 10. (wound closed). Tissue was stored in RNA later (for gene expression analysis) or embedded in OCT for immunofluorescence.

NFkB nuclear localisation

Cells were seeded in a 96-well dish (10000 cells/well) and were serum-starved overnight 24-hours later, followed by treatment with either buffer or Mindin. Post-treatment cells were fixed with 4% PFA, permeabilised and stained with NFkB (Santa Cruz SC372) antibody at 1:200 dilution. A secondary antibody (Jackson ImmunoResearch 711-545-152) was used at 1:200. A DAPI stain was used to mark nuclei. Images were captured with an Olympus IX73 microscope.

Immunofluorescence of skin sections

Skin tissues were fixed and sectioned as previously reported (15) and probed with the following antibodies diluted 1:200: K5 (Jamora lab previously described in Rana et al., 2023 (15), Badarinath et al., 2022 (18), Pincha et al., 2018 (49), Nakasaki et al., 2015 (36)); SCA1 (R&D AF1226); CD26 (R&D AF954); CD11b (Abcam ab8878); CD3 (e-biosciences 14-0032-85), F4/80 (e-biosciences 14-4801-81). aSMA (Abcam ab5694) was used at 1:50 dilution. Secondary antibodies (Jackson ImmunoResearch 711-545-152, 711-575-152, 712-545-150, 712-575-150, 703-545-155, 705-545-147, and Invitrogen A11055, A11057, A21208) were used at a 1:200 dilution. DAPI stain was used to mark nuclei. Images were captured with an Olympus IX73 microscope.

Gene set enrichment analysis (GSEA)

A Gene list was created using the upregulated genes with adjusted p-value(q)<0.05 and fold change > 1.5 from the RNAseq dataset of Mindin-treated human dermal fibroblasts described earlier (15). Database for Annotation, Visualisation and Integrated Discovery (DAVID) was used for GSEA (76–78). GOTERM_BP_Direct (79, 80) was used to visualise enriched biological processes, KEGG pathways (81) for identifying associated signalling pathways and the DisGeNET database for identifying the enrichment in associated diseases (82). Marker genes for different fibroblasts in keloids were extracted from Deng et al., 2021 (68). Gene overlap analysis was performed and Venn diagrams were created using Venny 2.0 (83).

Gene Expression

Total RNA was extracted from cells treated with either buffer or Mindin for 16-hours using TRIzol Reagent (TaKaRa, Thermo Fisher Scientific), and cDNA was synthesised using Superscript III (Thermo Fisher Scientific). The quantitative PCR (qPCR) was performed using Power SYBR Mix (Life Technologies, Thermo Fisher Scientific) in a Bio-Rad CFX384 machine. *Gapdh* or Actin (*Actb*) expression was used as a reference for normalisation. The primer sequences used are listed in Supplemental Table 6.

ELISA

The ELISA for IL-6 (Sigma RAB0306) and IL-1β (R&D DLB50) was performed on dermal fibroblasts treated with either Buffer, rMindin, conditioned media or IL-1α (as positive control) according to the manufacturer’s protocol.

Statistics

Welch's t-test was used for the comparison of the two groups. Ratio-paired t-test was used for comparison of fold changes in paired data. One-way ANOVA followed by Tukey's post hoc analysis was used for comparing three or more groups. 2-way ANOVA followed by post hoc Šídák's multiple comparisons test was used to compare three or more groups over multiple conditions. GraphPad Prism 6 (GraphPad Software) was used for all statistical

analyses. p-value for overlap between gene lists was calculated using a hypergeometric test available at http://nemates.org/MA/progs/overlap_stats.html. The data is represented as the mean ± SEM. P values of less than 0.05 were considered significant.

Study approval

Animal work conducted at the NCBS/inStem Animal Care and Resource Centre was approved by the inStem Institutional Animal Ethics Committee following the norms specified by the Committee for Control and Supervision of Experiments on Animals (Government of India). All experimental work was approved by the inStem Institutional Biosafety Committee (IBSC).

Data availability

The RNAseq data for Mindin-treated fibroblasts used in this study is deposited in NCBI SRA database BioProject accession ID: PRJNA846577 (https://www.ncbi.nlm.nih.gov/bioproject/PRJNA846577)

The supporting data values for graphs in the figures is provided in an excel file named - Supporting data values.

ACKNOWLEDGEMENTS

The authors would like to thank members of Jamora laboratory for their critical review of the work and insightful discussions, Ritoparna Hazra for designing the graphical model, and Achyuth Acharya for technical assistance. This work was supported by core funds from inStem, and grants from the Department of Biotechnology (DBT) of the Government of India (BT/PR8738/AGR/36/770/2013) and (BT/PR32539/BRB/10/1814/2019); the NIH/NIAMS (5R01AR053185-03); and the American Cancer Society (15457-RSG-08-164-01-DDC) to CJ. SK and KB were partially supported by the National Centre of Biological Sciences. IR was supported by the Indian Council of Medical Research (Senior Research Fellowship); Animal studies were partially supported by the National Mouse Research Resource (NaMoR) grant BT/PR5981/MED/31/181/2012;2013-2016;2018 and 102/IFD/SAN/5003/2017-2018 from the DBT. We thank the staff of the BLiSC Animal Care and Resource Centre and the BLiSC Central Imaging and Flow Cytometry Facility for technical assistance.

AUTHOR CONTRIBUTIONS

SK and CJ conceptualised and designed experiments, evaluated and interpreted data, and wrote the manuscript. SK, IR, KB, RFZ, GK, SA, AR, DS, RKZ, BD, AD, and EYH performed experiments. PK and SK performed bioinformatics analysis. AG provided resources and guidance for experimental design and analysis. CJ provided guidance and provided resources.

REFERENCES

1. Wynn TA. Cellular and molecular mechanisms of fibrosis. *J Pathol*. 2008;214(2):199–210.

2. Thannickal VJ, et al. Mechanisms of Pulmonary Fibrosis. *Annu Rev Med*. 2004;55(1):395–417.

3. Kendall RT, Feghali-Bostwick CA. Fibroblasts in fibrosis: novel roles and mediators. *Front Pharmacol*. 2014;5:123.

4. Thiruvoth FM, et al. Current concepts in the physiology of adult wound healing. *Plast Aesthetic Res*. 2015;2(5):250–256.

5. Bainbridge P. Wound healing and the role of fibroblasts. *J Wound Care*. 2013;22(8):407–412.

6. Wynn TA. Common and unique mechanisms regulate fibrosis in various fibroproliferative diseases. *J Clin Invest*. 2007;117(3):524–9.

7. Korosec A, et al. Lineage Identity and Location within the Dermis Determine the Function of Papillary and Reticular Fibroblasts in Human Skin. *J Invest Dermatol*. 2019;139(2):342–351.

8. Philippeos C, et al. Spatial and Single-Cell Transcriptional Profiling Identifies Functionally Distinct Human Dermal Fibroblast Subpopulations. *J Invest Dermatol*. 2018;138(4):811.

9. Driskell RR, et al. Distinct fibroblast lineages determine dermal architecture in skin development and repair. *Nature*. 2013;504(7479):277.

10. Mastrogiannaki M, et al. β-Catenin Stabilization in Skin Fibroblasts Causes Fibrotic Lesions by Preventing Adipocyte Differentiation of the Reticular Dermis. *J Invest Dermatol*. 2016;136(6):1130–1142.

11. Rinkevich Y, et al. Skin fibrosis. Identification and isolation of a dermal lineage with intrinsic fibrogenic potential. *Science*. 2015;348(6232). https://doi.org/10.1126/SCIENCE.AAA2151.

12. Suttho D, et al. 3D modeling of keloid scars in vitro by cell and tissue engineering. *Arch Dermatological Res 2016 3091*. 2016;309(1):55–62.

13. Nazari B, et al. Altered Dermal Fibroblasts in Systemic Sclerosis Display Podoplanin and CD90. *Am J Pathol*. 2016;186(10):2650.

14. Jamora C, et al. A Signaling Pathway Involving TGF-β2 and Snail in Hair Follicle Morphogenesis. *PLOS Biol*. 2004;3(1):e11.

15. Rana I, et al. Mindin (SPON2) Is Essential for Cutaneous Fibrogenesis in a Mouse Model of Systemic Sclerosis. *J Invest Dermatol*. 2023;143(5):699-710.e10.

16. Weeding E, Casciola-Rosen L, Shah AA. Cancer and scleroderma. *Rheum Dis Clin North Am*. 2020;46(3):551.

17. Du F, et al. Expression of Snail in Epidermal Keratinocytes Promotes Cutaneous Inflammation and Hyperplasia Conducive to Tumor Formation. *Cancer Res*. 2010;70(24):10080–10089.

18. Badarinath K, et al. Snail maintains the stem/progenitor state of skin epithelial cells and carcinomas through the autocrine effect of matricellular protein Mindin. *Cell Rep*. 2022;40(12):111390.

19. Piersma B, Hayward MK, Weaver VM. Fibrosis and cancer: A strained relationship. *Biochim Biophys acta Rev cancer*. 2020;1873(2):188356.

20. Kalluri R. The biology and function of fibroblasts in cancer. *Nat Rev Cancer 2016 169*. 2016;16(9):582–598.

21. Kalluri R, Zeisberg M. Fibroblasts in cancer. *Nat Rev Cancer*. 2006;6(5):392–401.

22. Geng X, et al. Cancer-Associated Fibroblast (CAF) Heterogeneity and Targeting Therapy of CAFs in Pancreatic Cancer. *Front Cell Dev Biol*. 2021;9. https://doi.org/10.3389/FCELL.2021.655152.

23. Murakoshi M, et al. Mindin: A novel marker for podocyte injury in diabetic nephropathy. *Nephrol Dial Transplant*. 2011;26(7):2153–2160.

24. Wang L, et al. Mindin is a critical mediator of ischemic brain injury in an experimental stroke model. *Exp Neurol*. 2013;247:506–516.

25. Murakoshi M, et al. Role of mindin in diabetic nephropathy. *Exp Diabetes Res*. 2011;2011. https://doi.org/10.1155/2011/486305.

26. Yang K, et al. Mindin deficiency alleviates renal fibrosis through inhibiting NF-κB and TGF-β/Smad pathways. *J Cell Mol Med*. 2020;24(10):5740.

27. Zhang C, et al. Mindin deficiency in macrophages protects against foam cell formation and atherosclerosis by targeting LXR-β. *Clin Sci (Lond)*. 2018;132(11):1199–1213.

28. Chiarelli N, et al. Cellular and Molecular Mechanisms in the Pathogenesis of Classical, Vascular, and Hypermobile Ehlers–Danlos Syndromes. *Genes (Basel)*. 2019;10(8). https://doi.org/10.3390/GENES10080609.

29. Moon MS, et al. Mindin, a Regulator of Innate Immunity and Inhibitor of Angiogenesis, Contributes to Mortality and Adverse Remodeling Post Myocardial Infarction. *J Card Fail*. 2009;15(6):S39.

30. Balakrishnan L, et al. Proteomic analysis of human osteoarthritis synovial fluid. *Clin Proteomics*. 2014;11(1):6.

31. Feng Y, et al. Upregulation of Spondin-2 protein expression correlates with poor prognosis in hepatocellular carcinoma. *J Int Med Res*. 2019;47(2):569–579.

32. Schmid F, et al. SPON2, a newly identified target gene of MACC1, drives colorectal cancer metastasis in mice and is prognostic for colorectal cancer patient survival. *Oncogene*. 2016;35(46):5942–5952.

33. Yuan X, et al. Spondin2 is a new prognostic biomarker for lung adenocarcinoma. *Oncotarget*. 2017;8(35):59324.

34. Ni H, et al. Spondin-2 is a novel diagnostic biomarker for laryngeal squamous cell carcinoma. *Pathol Res Pract*. 2019;215(2):286–291.

35. Parry R, et al. Identification of a novel prostate tumor target, mindin/RG-1, for antibody-

based radiotherapy of prostate cancer. *Cancer Res*. 2005;65(18):8397–8405.

36. Nakasaki M, et al. The matrix protein Fibulin-5 is at the interface of tissue stiffness and inflammation in fibrosis. *Nat Commun*. 2015;6. https://doi.org/10.1038/ncomms9574.

37. Zou ML, et al. Fibroblasts: Heterogeneous Cells With Potential in Regenerative Therapy for Scarless Wound Healing. *Front Cell Dev Biol*. 2021;9:1955.

38. Driskell RR, Watt FM. Understanding fibroblast heterogeneity in the skin. *Trends Cell Biol*. 2015;25(2):92–9.

39. Shaw TJ, Rognoni E. Dissecting Fibroblast Heterogeneity in Health and Fibrotic Disease. *Curr Rheumatol Rep*. 2020;22(8). https://doi.org/10.1007/S11926-020-00903-W.

40. Li H, et al. Efficient dendritic cell priming of T lymphocytes depends on the extracellular matrix protein mindin. *Embo J*. 2006;25(17):4097–4107.

41. Li Y, et al. Structure of the F-spondin domain of mindin, an integrin ligand and pattern recognition molecule. *EMBO J*. 2009;28(3):286–97.

42. Zhang YL, et al. Spon2 promotes m1-like macrophage recruitment and inhibits hepatocellular carcinoma metastasis by distinct integrin–rho gtpase–hippo pathways. *Cancer Res*. 2018;78(9):2305–2317.

43. Cary LA, Chang JF, Guan JL. Stimulation of cell migration by overexpression of focal adhesion kinase and its association with Src and Fyn. *J Cell Sci*. 1996;109(7):1787–1794.

44. Klinghoffer RA, et al. Src family kinases are required for integrin but not PDGFR signal transduction. *EMBO J*. 1999;18(9):2459–2471.

45. Zou L, et al. Fibronectin Induces Endothelial Cell Migration through β1 Integrin and Src-dependent Phosphorylation of Fibroblast Growth Factor Receptor-1 at Tyrosines 653/654 and 766. *J Biol Chem*. 2012;287(10):7190–7202.

46. Hanke JH, et al. Discovery of a Novel, Potent, and Src Family-selective Tyrosine Kinase Inhibitor: STUDY OF Lck- AND FynT-DEPENDENT T CELL ACTIVATION (∗). *J Biol Chem*. 1996;271(2):695–701.

47. Ma YC, et al. The Tyrosine Kinase c-Src Directly Mediates Growth Factor-Induced Notch-1 and Furin Interaction and Notch-1 Activation in Pancreatic Cancer Cells. *PLoS One*. 2012;7(3):e33414.

48. Brandvold KR, et al. Development of a highly selective c-Src kinase inhibitor. *ACS Chem Biol*. 2012;7(8):1393–1398.

49. Pincha N, et al. PAI1 mediates fibroblast–mast cell interactions in skin fibrosis. *J Clin Invest*. 2018;128(5):1807.

50. Barnes PJ, Karin M. Nuclear Factor-κB — A Pivotal Transcription Factor in Chronic Inflammatory Diseases. *https://doi.org/101056/NEJM199704103361506*. 1997;336(15):1066–1071.

51. Pantano C, et al. Nuclear Factor-κB Activation in Airway Epithelium Induces Inflammation and Hyperresponsiveness. *Am J Respir Crit Care Med*. 2008;177(9):959.

52. Tak PP, Firestein GS. NF-κB: a key role in inflammatory diseases. *J Clin Invest*.

2001;107(1):7–11.

53. Mu N, et al. A novel NF-κB/YY1/microRNA-10a regulatory circuit in fibroblast-like synoviocytes regulates inflammation in rheumatoid arthritis. *Sci Reports 2016 61*. 2016;6(1):1–14.

54. Nejatbakhsh Samimi L, et al. NF-κB signaling in rheumatoid arthritis with focus on fibroblast-like synoviocytes. *Autoimmun Highlights*. 2020;11(1). https://doi.org/10.1186/S13317-020-00135-Z.

55. Wang J, et al. The immune function of dermal fibroblasts in skin defence against pathogens. *Exp Dermatol*. 2023;32(9):1326–1333.

56. Cooper PO, et al. Dermal Drivers of Injury-Induced Inflammation: Contribution of Adipocytes and Fibroblasts. *Int J Mol Sci 2021, Vol 22, Page 1933*. 2021;22(4):1933.

57. Nakagawa S, Pawelek P, Grinnell F. Long-term culture of fibroblasts in contracted collagen gels: Effects on cell growth and biosynthetic activity. *J Invest Dermatol*. 1989;93(6):792–798.

58. Hu M, et al. Therapeutic Targeting of Src Kinase in Myofibroblast Differentiation and Pulmonary Fibrosis. *J Pharmacol Exp Ther*. 2014;351(1):87–95.

59. Zent J, Guo LW. Signaling Mechanisms of Myofibroblastic Activation: Outside-in and Inside-Out. *Cell Physiol Biochem*. 2018;49(3):848–868.

60. Karsdal MA, et al. The good and the bad collagens of fibrosis – Their role in signaling and organ function. *Adv Drug Deliv Rev*. 2017;121:43–56.

61. Rudnicka L, et al. Elevated expression of type VII collagen in the skin of patients with systemic sclerosis. Regulation by transforming growth factor-beta. *J Clin Invest*. 1994;93(4):1709–1715.

62. Galbo PM, Zang X, Zheng D. Implication of cancer associated fibroblast subtypes on cancer pathogenesis, prognosis, and immunotherapy resistance. *Clin Cancer Res*. 2021;27(9):2636.

63. Kieffer Y, et al. Single-cell analysis reveals fibroblast clusters linked to immunotherapy resistance in cancer. *Cancer Discov*. 2020;10(9):1330–1351.

64. Su S, et al. CD10+GPR77+ Cancer-Associated Fibroblasts Promote Cancer Formation and Chemoresistance by Sustaining Cancer Stemness. *Cell*. 2018;172(4):841-856.e16.

65. LeBleu VS, Kalluri R. A peek into cancer-associated fibroblasts: origins, functions and translational impact. *Dis Model Mech*. 2018;11(4). https://doi.org/10.1242/DMM.029447.

66. Sahai E, et al. A framework for advancing our understanding of cancer-associated fibroblasts. *Nat Rev Cancer 2020 203*. 2020;20(3):174–186.

67. Solé-Boldo L, et al. Single-cell transcriptomes of the human skin reveal age-related loss of fibroblast priming. *Commun Biol*. 2020;3(1). https://doi.org/10.1038/S42003-020-0922-4.

68. Deng CC, et al. Single-cell RNA-seq reveals fibroblast heterogeneity and increased mesenchymal fibroblasts in human fibrotic skin diseases. *Nat Commun*. 2021;12(1). https://doi.org/10.1038/S41467-021-24110-Y.

69. Gonsalves FC, et al. An RNAi-based chemical genetic screen identifies three small-molecule inhibitors of the Wnt/wingless signaling pathway. *Proc Natl Acad Sci U S A*. 2011;108(15):5954–5963.

70. Li X, et al. On the mechanism of long-range orientational order of fibroblasts. *Proc Natl Acad Sci U S A*. 2017;114(34):8974–8979.

71. Jia W, Li H, He YW. The extracellular matrix protein mindin serves as an integrin ligand and is critical for inflammatory cell recruitment. *Blood*. 2005;106(12):3854–3859.

72. Bhattacharjee S, et al. Tumor restriction by type I collagen opposes tumor-promoting effects of cancer-associated fibroblasts. *J Clin Invest*. 2021;131(11). https://doi.org/10.1172/JCI146987.

73. Nowak JA, Fuchs E. Isolation and culture of epithelial stem cells. *Methods Mol Biol*. 2009;482:215–232.

74. Bhatt T, et al. Initiation of wound healing is regulated by the convergence of mechanical and epigenetic cues. *Plos Biol*. 2022;20(9):e3001777–e3001777.

75. Pincha N, et al. Activation of Fibroblast Contractility via Cell-Cell Interactions and Soluble Signals. *Bio-protocol*. 2018;8(18). https://doi.org/10.21769/BIOPROTOC.3021.

76. Huang DW, Sherman BT, Lempicki RA. Systematic and integrative analysis of large gene lists using DAVID bioinformatics resources. *Nat Protoc*. 2009;4(1):44–57.

77. Huang DW, et al. The DAVID Gene Functional Classification Tool: a novel biological module-centric algorithm to functionally analyze large gene lists. *Genome Biol*. 2007;8(9):R183.

78. Huang DW, et al. DAVID Bioinformatics Resources: expanded annotation database and novel algorithms to better extract biology from large gene lists. *Nucleic Acids Res*. 2007;35(suppl_2):W169–W175.

79. Carbon S, et al. The Gene Ontology resource: enriching a GOld mine. *Nucleic Acids Res*. 2021;49(D1):D325.

80. Ashburner M, et al. Gene Ontology: tool for the unification of biology. *Nat Genet*. 2000;25(1):25.

81. Kanehisa M, Goto S. KEGG: Kyoto Encyclopedia of Genes and Genomes. *Nucleic Acids Res*. 2000;28(1):27.

82. Piñero J, et al. The DisGeNET knowledge platform for disease genomics: 2019 update. *Nucleic Acids Res*. 2020;48(D1):D845–D855.

83. Oliveros JC. Oliveros, J.C. (2007-2015) Venny. An Interactive Tool for Comparing Lists with Venn's Diagrams. - References - Scientific Research Publishing [Internet]. https://www.scirp.org/%28S%28czeh2tfqyw2orz553k1w0r45%29%29/reference/referencespapers.aspx?referenceid=2904043. Accessed May 25, 2022.

84. Preibisch S, Saalfeld S, Tomancak P. Globally optimal stitching of tiled 3D microscopic image acquisitions. *Bioinformatics*. 2009;25(11):1463–1465.

Figure 1:

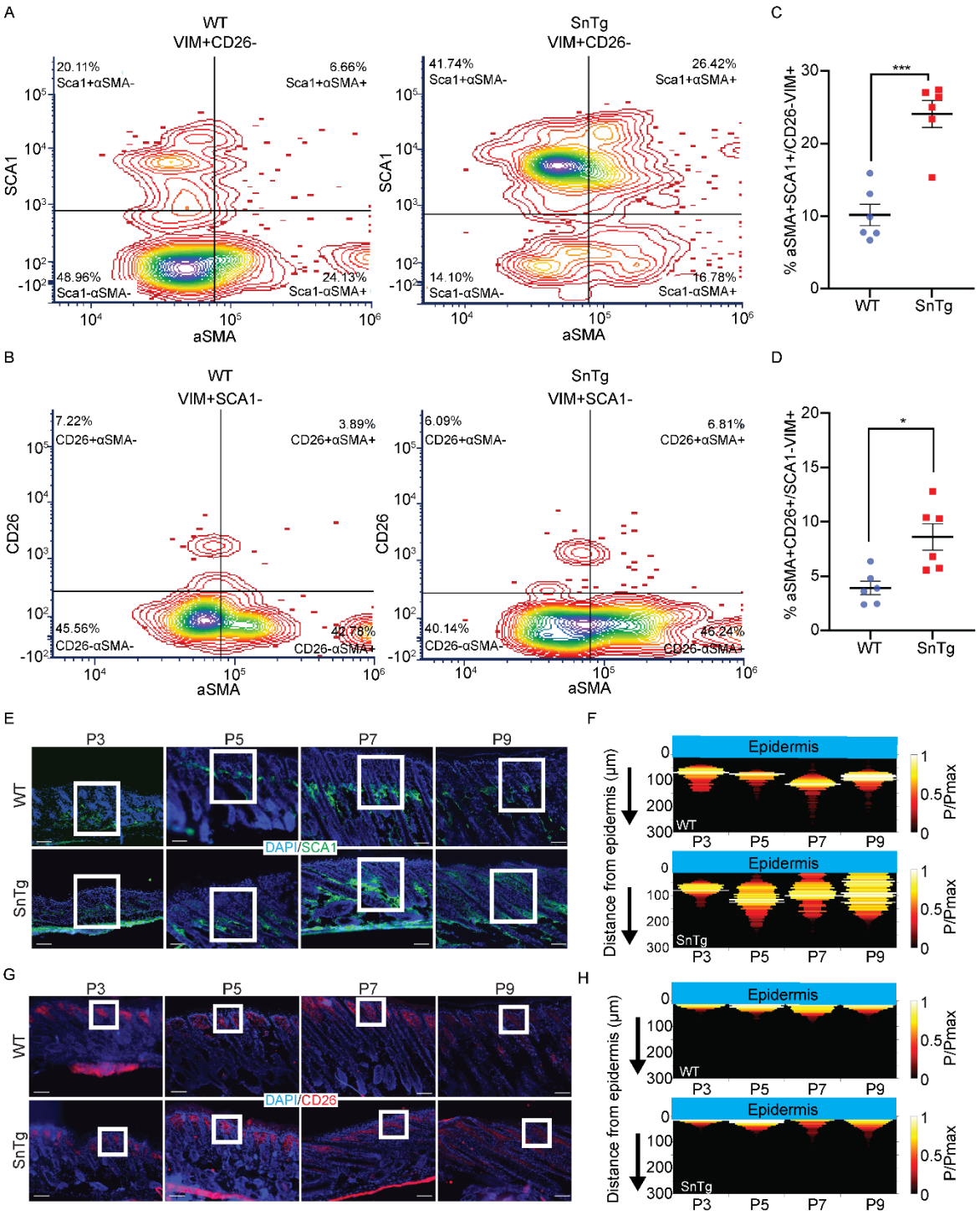

Figure 1: SCA1⁺ fibroblast localisation is perturbed in the dermis of *Snail transgenic* (*SnTg*) mice.

Representative contour plot showing quadrants for (A) aSMA±SCA1±/CD26-VIM^{High} cells and (B) aSMA±CD26±/SCA1-VIM^{High} cells, in postnatal day 9 (P9), WT (left panel) and *SnTg* (right panel). Individual value plot with mean±sem of (C) % aSMA⁺SCA1⁺/CD26-VIM^{High} and (D) % aSMA⁺CD26⁺/SCA1-VIM^{High} cells (n=6; p-values were calculated by Welch's t-test; *** p <

0.001, * p<0.05). (E) SCA1^{+} fibroblasts (green) and nuclear staining with DAPI (blue) in WT and *SnTg* skin sections in postnatal day 3 (P3), P5, P7 P9 pups. The white box marks the inset shown in Figure S1J. Note that the green stain at the bottom of the skin section is the autofluorescence of the paper used to keep the tissue uncurled during the embedding process. (F) Heatmap showing the probability of SCA1^{+} cells at a given distance below the epidermis in WT (top panel) and *SnTg* (Bottom panel) mice P3 (n=3 WT and *Snail Tg*), P5 (n=2 WT and n=4 *Snail Tg*), P7 (n=3 WT and n=4 *Snail Tg*), and P9 (n=6 WT and n=8 *Snail Tg*). (G) CD26^{+} fibroblasts (red) and nuclear staining with DAPI (blue) in WT and *SnTg* skin sections from P3, P5, P7, and P9 pups. The white box marks the insets shown in Figure S1L as magnified areas. Note that the red stain at the bottom of the skin section is the autofluorescence of the paper used to keep the tissue uncurled during the embedding process. (H) Heatmap showing the probability of CD26^{+} cells at a given distance below the epidermis in WT (top panel) and *SnTg* (Bottom panel) at P3 (n=2 WT and n=3 *Snail Tg*), P5 (n=2 WT and n=3 *Snail Tg*), P7 (n=3 WT and n=3 *Snail Tg*), and P9 (n=4 WT and n=6 *Snail Tg*).

Figure 2:

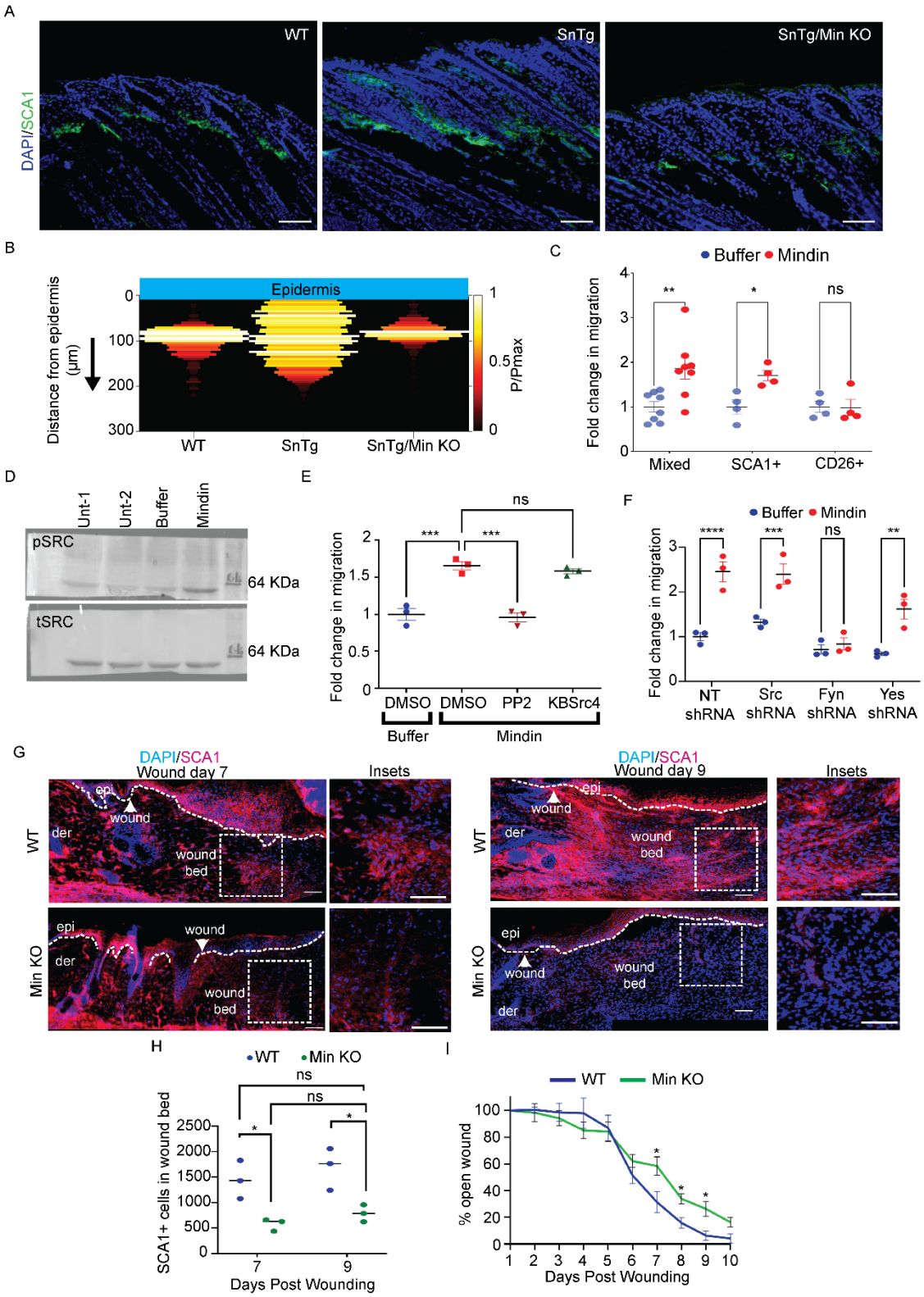

Figure 2: Mindin induces migration of SCA1⁺ fibroblasts via Fyn kinase (A) IF staining for SCA1 in P9 WT, *SnTg* and *SnTg/Mindin knockout* (*Min KO*) skin (scale bar = 50 μm). (B) Heatmap showing the probability of SCA1⁺ cells at a given distance below the epidermis in

WT (n=6), *SnTg* (n=8) and *SnTg/Min KO* (n=4) skin. WT and *SnTg* are the same data as in Figure 1F. (C) Transwell assay to measure migration of mixed, $SCA1^+$ and $CD26^+$ fibroblasts with either buffer or Mindin as a potential chemoattractant (n≥4). (D) Amount of phosphorylated SRC (pSRC) and total SRC proteins (tSRC) in fibroblasts treated with either buffer or Mindin for 15 minutes. (E) Transwell assay with $SCA1^+$ fibroblasts stimulated with buffer or Mindin in the presence of DMSO, PP2 (10 μM), or KbSrc4 (10 μM) (n=3). (F) Transwell assay with. $SCA1^+$ fibroblasts transduced with either Non-targeting (NT), *Src*, *Fyn* or *Yes* shRNA with buffer or Mindin as a chemoattractant (n=3). (G) IF for SCA1, in WT and *Min KO* day-7 and day-9 skin wounds (The images were stitched using FIJI ImageJ stitching tool (84); scale bar = 50 μm). The white box shows the region marked for inset magnified on the right-hand side of each image (H) Quantification of SCA1+ cells in the wound beds day-7 and day-9 post-wounding of WT and *Min KO* mice (n=3 mice) (I) Percent wound closure in WT and *Min KO* mice w.r.t. wound size on day 1. (n = 3 mice, 2 wounds per mice). Data represent the mean ± SEM. p-values were calculated by Welch's t-test (C and I), 1-way ANOVA followed by Tukey's post hoc analysis (E), 2-way ANOVA followed by post hoc Šídák's multiple comparisons test (F and H) (*p<0.05, **p<0.01, ***p< 0.001, ****p <0.0001 and ns (p>0.05) is non-significant).

Figure 3:

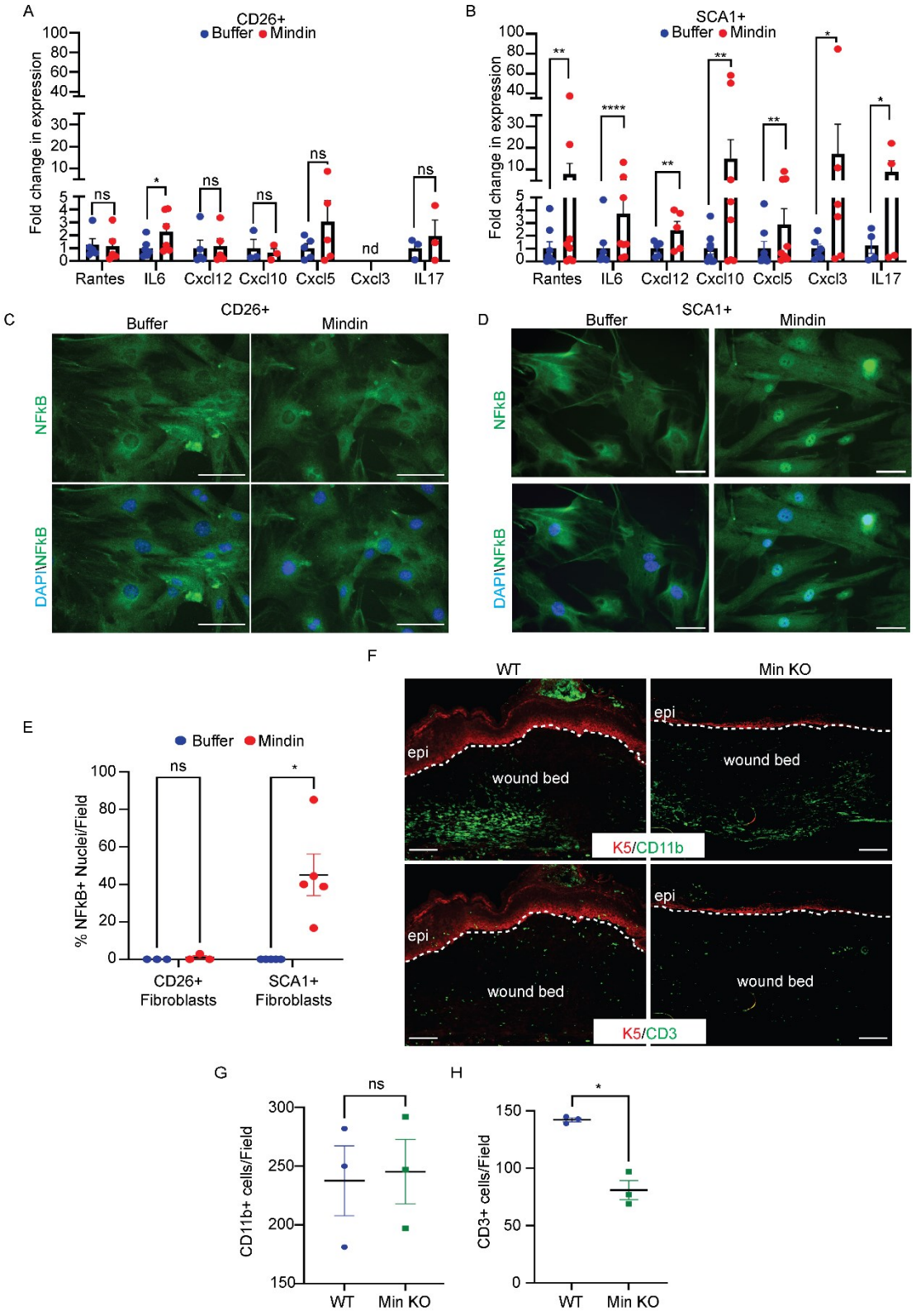

Figure 3: Mindin stimulates inflammatory cytokine production in SCA1⁺ fibroblasts
qPCR for expression of inflammatory cytokines from (A) CD26⁺ fibroblasts or (B) SCA1⁺ fibroblasts treated with either buffer or Mindin (n≥4). Staining for NFkB(green) and DAPI

(blue) in (C) $CD26^+$ fibroblasts or (D) $SCA1^+$ fibroblasts treated for 1-hour with either buffer or Mindin and (E) and percentage of cells with NFkB+ nuclei per field in CD26+ (n=3) or SCA1+ (n=5) fibroblast treated with either buffer or Mindin. (F) IF staining for K5(red) and CD11b (top panel; green; macrophages) and CD3 (bottom panel; green; T-Cells) in WT and *Min KO* skin sections post-wounded day 7 (scale bar = 50 μm) and quantification of (G) $CD11b^+$ and (H) $CD3^+$ cells found in the wound bed (n=3 mice) Data represents the mean ± SEM. p-values were calculated by Ratio paired t-test (A and B) and Welch's t-test (E, G, H) (*p<0.05, **p<0.01, ***p<0.001, ****p<0.0001 and ns (p>0.05) is non-significant and nd=not detected).

Figure 4:

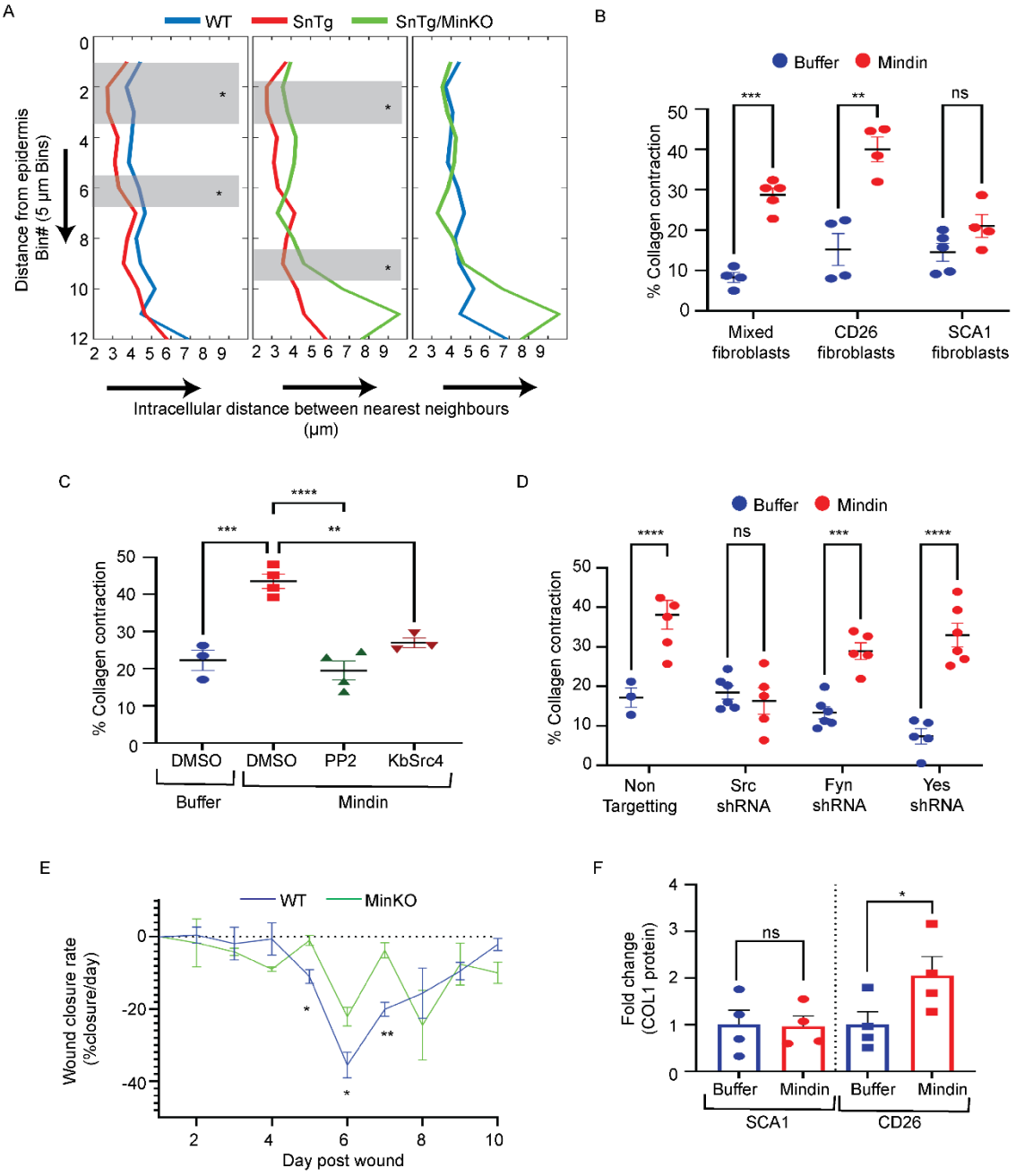

Figure 4. Mindin induces fibroblast contraction and collagen production in CD26⁺ fibroblasts. (A) Measurement of intracellular distance between two nearest CD26⁺ nuclei (x-axis) as a function of distance below the epidermis (y-axis, bin# below the epidermis, bin size = 5 µm) in WT, *SnTg* and *SnTg/Min KO* skin. (n = 3. The number of CD26⁺ cells counted per skin section > 80. The region shaded in grey marks the bins where $p<0.05$, calculated using Welch's t-test) (B) Collagen contraction assay, showing percentage contraction of collagen gels seeded with either mixed, CD26⁺, or SCA1⁺ fibroblasts and treated with either buffer control or Mindin (n≥4). (C) Effect of SFK inhibition on Mindin-induced collagen contraction. CD26⁺ fibroblasts were treated with either buffer control or Mindin along with either DMSO, PP2, or KbSrc4 (n≥3). (D) Effect of Non-targeting (NT), *Src*, *Fyn*, or *Yes* shRNA on collagen contraction with CD26⁺ fibroblasts, treated with either buffer control or Mindin

(n≥3). (E) Measurement of the rate of closure (slope) in WT and *Min KO* mice. The slope was calculated as % closure of a given day - % closure on the previous day (n = 3 mice, 2 wounds per mouse). (F) Quantification of COL1 in buffer control or Mindin-treated $CD26^+$ and $SCA1^+$ fibroblasts, normalised to Lamin B1 (LAM) (n=4). Data represent the mean±SEM. p values were calculated by Welch's t-test (B, E), ratio-paired t-test (F), 1-way ANOVA followed by Tukey's post hoc analysis (C), 2-way ANOVA followed by post hoc Šídák's multiple comparisons test (D) (*p < 0.05, **p < 0.01, ***p < 0.001, ****p < 0.0001 and ns (p>0.05) is non-significant).

Figure 5:

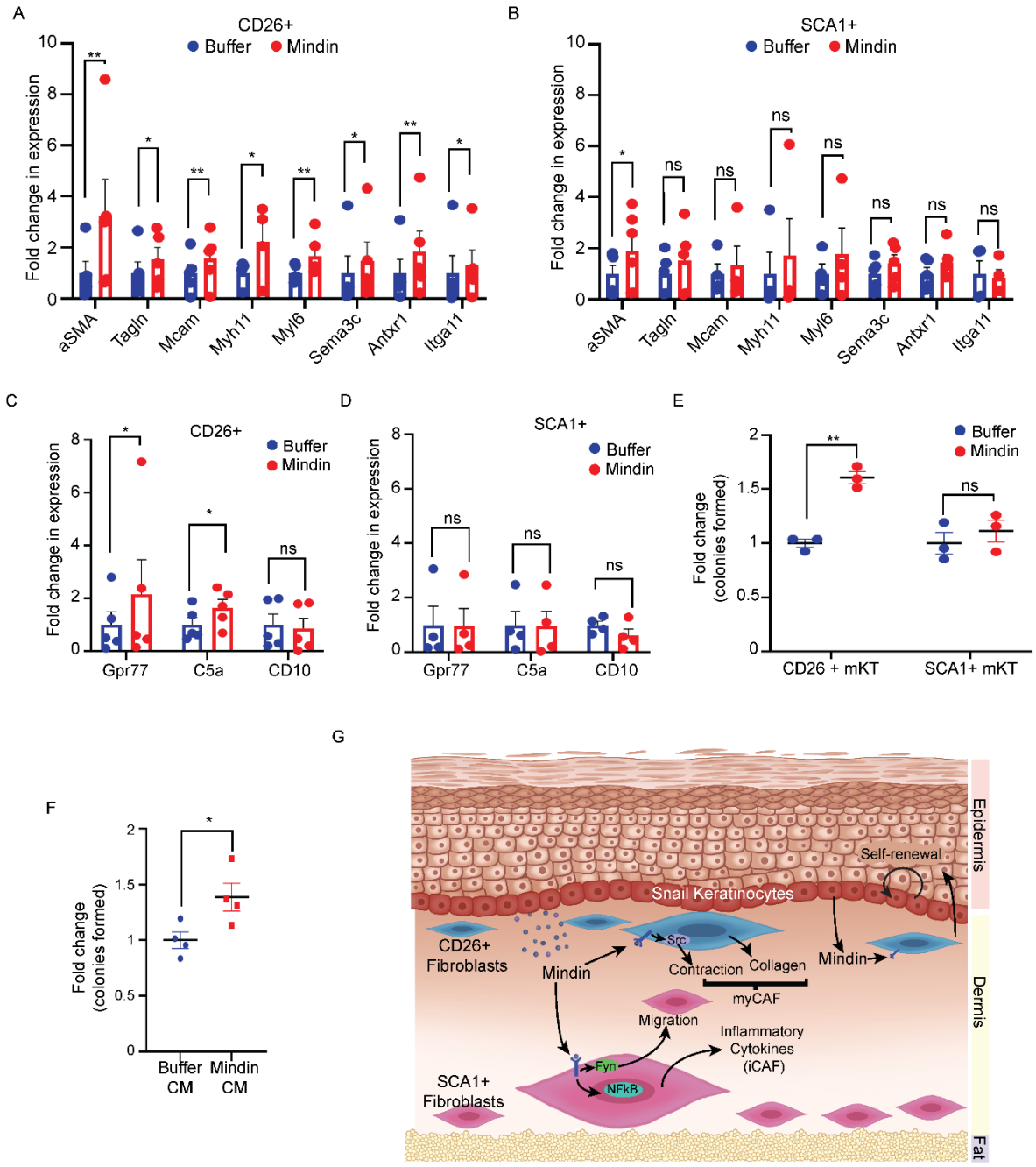

Figure 5: Mindin promotes CD26⁺ fibroblasts to adopt a CAF phenotype. qPCR for expression of signature genes of myCAFs in (A) CD26⁺ fibroblasts or (B) SCA1⁺ fibroblasts treated with either buffer or Mindin (n≥4). Expression of genes measured by qPCR that are associated with stem cell renewing CAFs in (C) CD26⁺ (n=6) and (D) SCA1⁺ (n=4) fibroblasts treated with either buffer of Mindin. (E) Colony formation assay of primary mouse keratinocytes (mKT) co-cultured with CD26⁺ or SCA1⁺ fibroblasts pre-treated with either buffer of Mindin for 24-hours (n=3). (F) Colony formation assay of primary mouse keratinocytes cultured with conditioned media (CM) collected from CD26⁺, fibroblasts treated with either buffer of Mindin (n=4). Data represent the mean ± SEM. p values were calculated by ratio

paired t-test (A-D), Welch’s t-test (E-F), (*p < 0.05, **p < 0.01, ns (p>0.05) is non-significant). (G) Model of differential effects of Mindin on distinct subpopulations of dermal fibroblasts.